

ORIGINAL ARTICLE

Domain morphology of newly designed lead-free antiferroelectric $\text{NaNbO}_3\text{-SrSnO}_3$ ceramicsHui Ding^{1,2}  | Mao-Hua Zhang³  | Jurij Koruza³  | Leopoldo Molina-Luna¹  | Hans-Joachim Kleebe²

¹Department of Materials and Earth Sciences, Advanced Electron Microscopy, Technical University of Darmstadt, Darmstadt, Germany

²Institute of Applied Geosciences, Geomaterial Science, Technical University of Darmstadt, Darmstadt, Germany

³Department of Materials and Earth Sciences, Nonmetallic Inorganic Materials, Technical University of Darmstadt, Darmstadt, Germany

Correspondence

Hui Ding, Institute of Applied Geosciences, Geomaterial Science, Technical University of Darmstadt, Darmstadt, Germany.
Email: hding@aem.tu-darmstadt.de

Funding information

Hessian State Ministry for Higher Education, Research and the Arts; Horizon 2020 European Research Council, Grant/Award Number: 805359-FOXON

Abstract

Reversible antiferroelectric-ferroelectric phase transitions were recently observed in a series of SrSnO_3 -modified NaNbO_3 lead-free antiferroelectric materials, exhibiting well-defined double polarization hysteresis loops at ambient conditions. Here, transmission electron microscopy was employed to investigate the crystallography and domain configuration of this newly designed system via electron diffraction and centered dark-field imaging. It was confirmed that antiferroelectricity is maintained in all compositions, manifested by the characteristic $\frac{1}{4}$ superlattice reflections in the electron-diffraction patterns. By investigating the antiferroelectric domains and domain boundaries in NaNbO_3 , we demonstrate that antiphase boundaries are present and their irregular periodicity is responsible for the streaking features along the $\frac{1}{4}$ superlattice reflections in the electron-diffraction patterns. The signature domain blocks observed in pure NaNbO_3 are maintained in the SrSnO_3 -modified ceramics, but disappear when the amount of SrSnO_3 reaches 7 mol.%. In particular, a well-defined and distinct domain configuration is observed in the NaNbO_3 sample modified with 5 mol.% SrSnO_3 , which presents a parallelogram domain morphology.

KEYWORDS

TEM, lead-free antiferroelectrics, sodium niobate, domain morphology, antiphase boundary

1 | INTRODUCTION

Antiferroelectric (AFE) materials draw worldwide attention due to their substantial potential in engineering applications, such as energy-storage capacitors or electrocaloric cooling devices.¹⁻³ The concept of “antiferroelectricity” was first coined by Kittel,⁴ followed by an extensive investigation of prototype lead zirconate-based solid solutions.⁵⁻⁸ Nowadays, lead-free AFE materials have gained increasing interest, driven by the intensive research on lead-free piezoelectric materials^{9,10} concerning the severe environmental and health issues with respect to the toxicity of lead-containing materials.¹¹

One of the prototype lead-free AFE materials is NaNbO_3 (NN), which was first reported in 1949 and was extensively investigated since then.¹²⁻¹⁷ At ambient conditions, the AFE phase of pure NN is commonly referred to as the *P* phase, with an orthorhombic *Pbma* space group.¹⁸ However, an additional ferroelectric phase, the *Q* phase with the orthorhombic space group *P2₁ma*,¹⁸ can be induced out of the *P* phase by application of electric field¹⁹ and change in grain size.²⁰ The *Q* phase was reported to coexist with the *P* phase at room temperature^{16,21,22} due to their minimal difference in free energy.^{23,24} It was recently reported that NN ceramics are characterized by a irreversible AFE-FE phase

This is an open access article under the terms of the Creative Commons Attribution-NonCommercial-NoDerivs License, which permits use and distribution in any medium, provided the original work is properly cited, the use is non-commercial and no modifications or adaptations are made.

© 2021 The Authors. *Journal of the American Ceramic Society* published by Wiley Periodicals LLC on behalf of American Ceramic Society (ACERS)

transition.¹⁹ Characteristic double hysteresis loop was only observed in few single crystals along specific crystallographic orientations.¹⁴ To enable the reversible field-induced AFE-FE phase transition, chemical modifications have been widely employed to stabilize the antiferroelectricity against ferroelectricity by lowering the Goldschmidt tolerance factor, as reported for several NN-based solid solutions.^{23,25,26} Recently, a new NN-based solid solution modified by SrSnO₃ has been developed by altering the free energy guided by first-principle calculations, characterized by a well-defined double hysteresis loop and strongly enhanced energy storage density (8-times higher) as compared to pure NN.²⁴

The study of the domain structure of NN single crystals was initiated in the early 1950s by the approach of optical microscopy, shortly after the discovery of the antiferroelectricity in NN.²⁷⁻²⁹ The domains were generally observed to form complex multi-domain structures in the crystal.²⁸ In the 1980s, it was concluded that only 90° and 60° domains were allowed in orthorhombic NN by the crystallographic symmetry.^{21,30} In the late 1980s, (transmission) electron microscopy has started to play an important role in visualizing the 90° and 60° domains in both NN single crystals and polycrystalline ceramics.³¹⁻³³ Since the 21st century, the rapid development of transmission electron microscopy (TEM) has enabled its wide application in the investigation of the domain structures. It has been established that pure NN ceramic has a hierarchical domain configuration, including signature micrometer-sized domain blocks and characteristic ¼ superlattice reflections of the AFE phase in the reciprocal space.²⁵ The observed lines with dark contrast were claimed to be translational domain walls, separating the translational domains.²⁵ Moreover, the streaking feature in the electron-diffraction patterns was believed to be associated with incommensurate structures.³⁴ However, after reviewing the fundamental theory of AFE materials compared to ferroelectric (FE) materials³⁵, we think the concept of domain walls needs either correction or further clarification. It is known that the antiparallel polarizations (antipolarization) in AFE crystals cancel each other, providing no electrostatic interaction during the AFE domain growth upon cooling from the high-temperature cubic phase. In other words, the concept of “domain walls” developed in FE materials (reduction of depolarizing fields and balancing the electrostatic interaction or mechanical energy), partially does not fit in the concept of AFE. Correspondingly, the term “translational domain walls” should also be revised.

Moreover, incommensurate structures are frequently observed in lead-containing AFE materials and characterized by the non-integer superlattice reflections in the electron-diffraction patterns.^{36,37} However, no such irrational superlattice reflections have been reported in the P phase of NN at ambient conditions, only at elevated temperatures of 165°C and 420°C.³⁸ On the other hand, the appearance of the streaking feature is not necessarily associated with the

incommensurate structures. Such streaking feature was observed in the commensurate AFE phase of (Pb, La)(Zr, Ti)O₃, which was attributed to either the strains rising from the intergrowth of different structural modulations or irregularities in the commensurate structures induced by impurities.^{36,39}

In this work, we carried out a systematic TEM study of the newly designed NN-based AFE solid solution (1-x)NaNbO₃-xSrSnO₃²⁴ by bright field and centered dark-field imaging in conjunction with electron diffraction. We initially demonstrate the typical domain morphology and crystallography of pure NN ceramic, elucidated with an updated concept of domain boundary (compared to the domain wall in ferroelectrics) and antiphase boundaries (APBs) in the realm of AFE materials. Then, we validate the antiferroelectric nature of the new solid solution by the presence of characteristic superlattice reflections in reciprocal space and reveal the domain configuration via bright-field and dark-field imaging.

2 | EXPERIMENTAL PROCEDURES

The (1-x)NaNbO₃-xSrSnO₃ ceramics (x = 0, 0.03, 0.05, and 0.07, where pure NaNbO₃ and SrSnO₃-modified samples are abbreviated as NN and NN-xSS, respectively) were prepared by the solid-state reaction route. NN-xSS powders were compacted into green bodies and were subjected to cold isostatic pressing with 200 MPa. The green bodies were sintered in the temperature range of 1330-1355°C for 2 hours in air. Sintered samples were ground to a thickness of 0.25 mm and were sputtered with Pt electrode. The electroded samples were annealed at 400°C and were cut into dimensions of 2 × 1.5 × 0.25 mm³ for electrical characterizations. Scanning electron microscopy (SEM, XL 30 FEG, Philips, Eindhoven, Netherlands) was used to characterize the microstructure of the sintered samples. Detailed descriptions of the synthesis, microstructure, and electrical characterizations can be found elsewhere.²⁴

For TEM sample preparation, thin cross sections of the as-sintered samples were polished down to a thickness of 20 μm using the MultiPrep polishing system (Allied High Tech Products Inc., USA) and diamond lapping films with grain sizes ranging from 15 μm to 1 μm. Subsequently, the samples were annealed at 400°C for 30 min to release the mechanical stress that may have been introduced during the preparation steps. Later, the thin sections were mounted on supporting molybdenum TEM grids (100 mesh; Plano, Germany) and Ar-ion milled using the DuoMill 600 (Gatan, USA) until electron transparency was reached. Finally, the TEM samples were lightly carbon-coated (Med 010; Liechtenstein) to minimize charging under the incident electron beam. It should be noted that all zone axes of the electron-diffraction patterns are arbitrarily indexed with respect to the pseudocubic NN unit cell. The TEM studies were performed with a JEM 2100F microscope (JEOL, Japan) operating at 200 keV. To

examine the twinning behavior, SAED patterns of each domain and domain boundary are taken with a camera length of 50 and 150 cm, respectively.

3 | RESULTS AND DISCUSSION

3.1 | Electrical properties

Polarization hysteresis loops of the investigated samples in the second electric field cycle are shown in Figure 1. The NN sample exhibits a square-like polarization hysteresis loop, which is a fingerprint of the irreversible field-induced AFE-FE phase transition.¹⁹ In contrast, double polarization hysteresis loops, which are a characteristic for AFEs with reversible transitions, are observed for SrSnO₃-modified samples NN-0.03SS and NN-0.05SS. This indicates that AFE order can be at least partially maintained after the samples are subjected to an electric field. Note that polarization hysteresis loops were not obtained for NN-0.07SS, due to the fact that the critical field required to induce the phase transition was higher than the sample's breakdown strength. The microstructures of the investigated samples are shown in Figure 2. The average grain size of NN is 8.9 μm, whereas the average grain sizes of 10.7 μm and 8.1 μm were determined for NN-0.03SS and NN-0.05SS, respectively.

3.2 | TEM characterization of pure NN

The TEM analysis was first carried out on pure NN, which served as the benchmark AFE material. In our previous studies in conjunction with ²³Na solid-state nuclear magnetic resonance investigations,²⁴ only the P phase was present in the virgin state (prior to the application of electric field).¹⁹ The NbO₆ octahedron tilting system in the P phase can be described by the Glazer notation, denoted as $a^-b^+a^-$ and $a^-b^-a^-$ ^{40,41} for the upper and lower parts of the structure, respectively. The top two layers of octahedra along the y

axis are paired by a (010) mirror plane, leading to a parallel displacement configuration, followed by an antiparallel displacement in the bottom two layers. Therefore, the unit cell is quadrupled along the [010] direction in the P phase.²⁹ Correspondingly, the multicell crystal structure of the P phase is characterized by the $\frac{1}{4}$ type superlattice reflections in the reciprocal space of the pseudocubic structure.²⁹

The antiferroelectricity of pure NN at room temperature is confirmed by the characteristic $\frac{1}{4}$ superlattice reflections in the electron-diffraction pattern (Figure 3B), denoted by the arrows. By using one of these $\frac{1}{4}$ superlattice reflections for centered dark-field imaging, the signature of the micrometer-sized domain blocks can be observed (width ranging from 0.5 to 0.9 μm, based on several images in this region; see Appendix Figure S1), which are marked by the blue dashed lines in Figure 3A. It should be pointed out that the entire grain is composed of such domain blocks, which, however, is not shown in Figure 3, due to the limitations of low magnification imaging. The parallel straight lines with dark contrast marked by the white line, are considered as antiphase boundaries (APBs), which are commonly reported in lead-containing AFE systems.⁴²⁻⁴⁴ In the classical view, APBs are manifested as interfaces, where the lattice structure on either side is perfect, and can be related by a translation operation with a displacement vector of half a lattice parameter, typically $\frac{1}{2}(a+b)$.⁴⁵ Note that such a definition of APBs is applicable to non-ferroics. The lattice periodicity in ferroics concerns not only the lattice structure, but also the identity of atomic displacements within the unit cell structure. Therefore, APBs in ferroics are treated as an area with finite thickness, separating the translational domains on both sides.⁴⁶ When we zoom into such a domain block, as shown in Figure 3B, the lattice fringes with a modulation length of approximately 1.6 nm along the [101] direction become visible, associated with the APBs. In Figure 3C, the HRTEM image reveals clearly the 4-layer multicell structure, separated by one additional atomic layer. This is consistent with a recent study on lead zirconate AFE ceramic, where APBs were characterized in HRSTEM

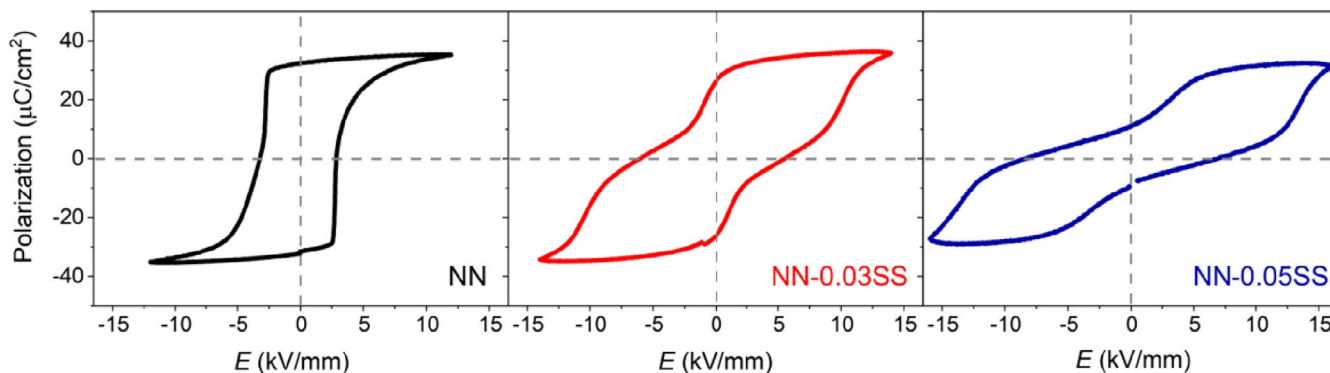


FIGURE 1 Polarization hysteresis loops of pure NN, NN-0.03SS, and NN-0.05SS, respectively [Color figure can be viewed at wileyonlinelibrary.com]

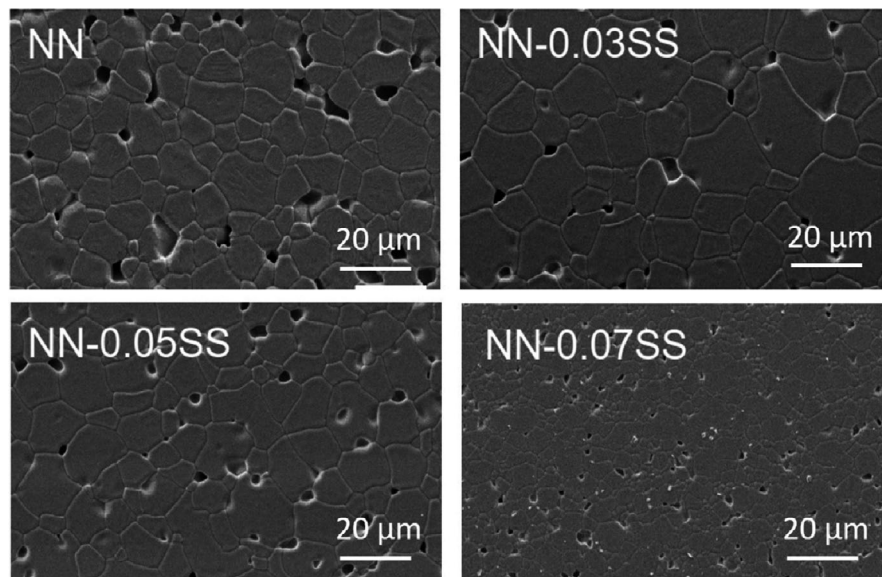


FIGURE 2 Microstructures characterized by scanning electron microscopy (SEM) of pure NN, NN-0.03SS, NN-0.05SS, and NN-0.07SS, respectively

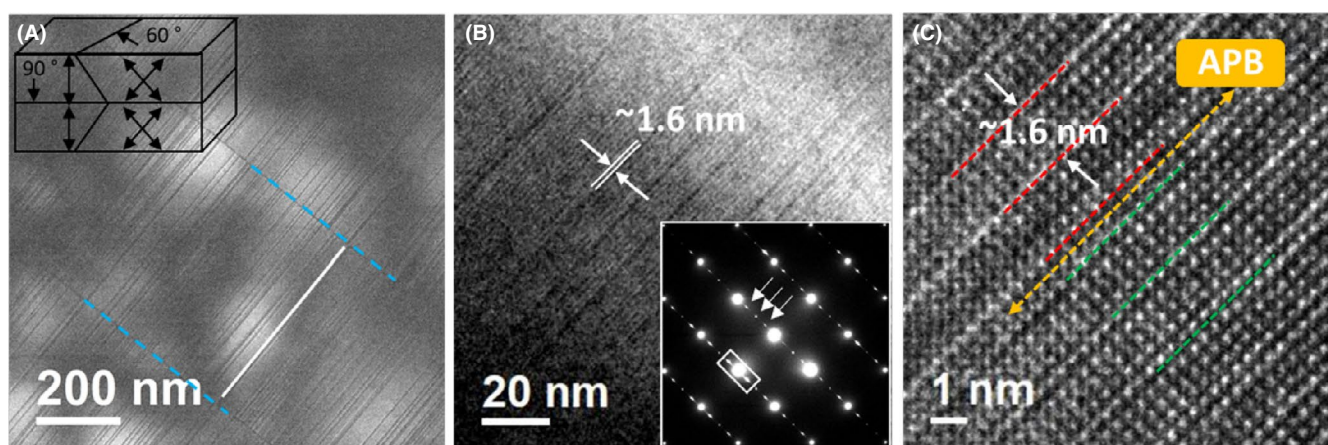


FIGURE 3 TEM characterization of the crystallography and domain morphology of one representative grain in pure NN ceramic. (A) centered dark-field (CDF) image obtained with one of the $\frac{1}{4}$ superlattice reflections marked by the white arrows in the selected-area electron-diffraction (SAED) pattern inserted in (B) with [010] orientation. Here the blue and white dashed lines denote the domain and antiphase boundaries (APBs), respectively. The inset model shows schematically 90° and 60° domains, drawn after Zhelnova et al.³³ Note that in (B) lattice fringes denoted by the white lines with a modulation length of about 1.6 nm associated with arrays of APBs (dark lines) are visible. The white square in the SAED pattern encloses the streaking feature around the $\frac{1}{4}$ superlattice reflections along [101] direction. (C) The high-resolution TEM (HRTEM) image, revealing a four-layer multicell structure with a modulation length of about 1.6 nm, separated by the orange line (APB), manifested by one atomic layer. The red and green dashed lines denote the multicell structures on both sides of the APB, respectively [Color figure can be viewed at wileyonlinelibrary.com]

imaging by 1-layer or 3-layers stripes, interrupting the rigid periodic arrangement of the multicell structure.⁴⁷ Therefore, it can be concluded that the multicell structure appears as lattice fringes, separated by APBs which appear as dark lines at a medium-high magnification (Figure 3B). The electron-diffraction pattern given in Figure 3B also reveals that the $\frac{1}{2}$ superlattice reflection spots originating from the oxygen octahedron tilting are round and well defined. On the other hand, the $\frac{1}{4}$ superlattice reflection spots are characterized by an obvious streaking feature, which was also observed in a commensurate orthorhombic AFE (Pb, La)(Zr, Ti)O₃ ceramic material, where the corresponding lattice image also reveals structural modulations of various periodicity.³⁶ It was

pointed out in the literature that the streaking feature is always present when there are structural modulations of various periodicity, but appears very weak (or disappears) when the lattice images show uniform spacing between fringes which are incommensurate with the lattice.³⁹ Therefore, we propose that the irregular periodicity of APB arrays is responsible for the streaking feature, in contrast to a previously reported incommensurate phase.³⁴ Note that no evidence for irrational superlattice reflections was observed in this work.

It is known that AFE domains are non-polar due to the cancellation of antipolarizations. When domains with equivalent crystallographic antipolarization directions meet and form a boundary, mechanical stress is released. Correspondingly,

domains in AFE were previously described as “mechanical twins” since twinning is the main approach in many ceramics to release mechanical stresses.^{21,35,48} As mentioned previously, there are only 90° and 60° twin domains in orthorhombic NN.³⁰ Thus, domain blocks with the same antipolarization direction will form a 90° twin wall (denoted by the blue dashed lines in Figure 3A), which is schematically shown in the inset model in Figure 3A.

Another representative grain with orientational domains is investigated in Figure 4A-C. When each domain takes equivalent but different antipolarization directions independently upon cooling from the paraelectric phase, they together as an ensemble are referred to as orientational domains. In order to reveal the specifics of the domain morphology of the orientational domains (with different diffraction contrast) simultaneously, the direct beam and the surrounding superlattice reflections were selected for the BF imaging, which is schematically denoted by the white circle shown in Appendix (Figure S2A). From the BF image viewed along the [121] direction (Figure 4A), orientational domains are displayed, where the antipolarization in each domain is denoted by a double-headed arrow. The domain configuration can also be recognized by the different orientations revealed in the electron-diffraction patterns with the same [121] zone axis. The characteristic ¼ superlattice reflections confirm the antiferroelectric nature unambiguously. By using one of these ¼ superlattice reflections, the irregular periodicity of the APB arrays is illustrated in both domains in the centered dark-field image, consistent with the streaking observed in the diffraction patterns. The APB nature is further confirmed by the existence of the intensities between the lines in the line profile (Figure S2E), which is in agreement with the situation depicted in Figure 3B. The line profiles, together with the details of the domain structures in domain 1 and 2, are given in the Appendix (Figure S2).

As pointed out in the introduction, the term domain wall (DW) is to some extent different in AFE from that in FE. In FE, domain splitting is commonly the result of the reduction in the electrostatic or mechanical energy.^{35,49} In AFE, however, domains experience no electrostatic interaction during the growth. Therefore, the mechanism of the formation of DWs in FE partially fails to describe the AFE behavior. Instead, the term domain boundary (DB) or twin boundary (TB) in terms of twinned domains would be a more accurate way for the description of AFE. The domain boundary between the upper and lower domain shown in Figure 4A is determined to be a 60° DB,³¹ which is also depicted in the schematic diagram in Figure 3A, originating from the intersection of the out-of-plane antipolarization orientations. This can also be explained by the diffraction contrast between the two domain variants, as indicated in the centered dark-field images (see Figure S2B and C). Upon projection, the domain variants appear perpendicular to each other.

To briefly summarize, both domain blocks as a result of the reduction of mechanical stresses and orientational domains as a result of taking different equivalent antipolarization directions independently (allowed by the symmetry) are observed in pure NN ceramic. Such domain configuration is expected to be the fundamental unit in NN-based solid solutions.

3.3 | TEM characterization of NN-SS

After the investigation of pure NN as a benchmark material, SrSnO₃-modified NN samples in the virgin state will be investigated in this section. When 3% SrSnO₃ is introduced into NN, the overall domain morphology such as domain blocks is preserved, as shown in Figure 5. As can be seen from the BF image in Figure 5A, the grain is composed

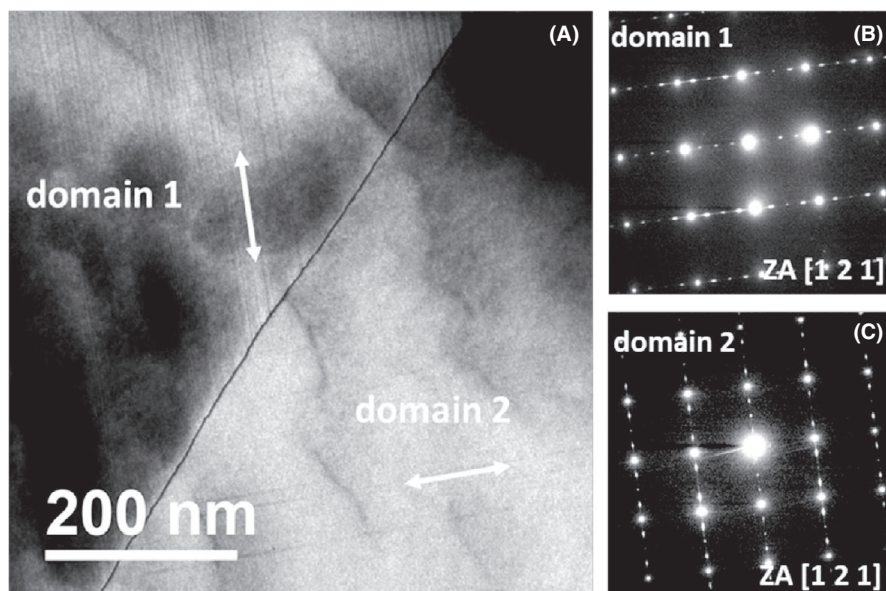


FIGURE 4 TEM characterization of the crystallography and domain morphology of another representative grain in pure NN ceramic. (A) Bright-field (BF) image viewed along the $\langle 121 \rangle$ direction, obtained with the direct beam and the surrounding ¼ reflections in the SAED pattern, taken at the domain boundary; the SAED patterns shown in (B) and (C) correspond to the upper and lower domains both oriented in the [121] zone axis with a 90° rotation, respectively

of several orientational domains (separated by the orange lines), as also recognized by the different orientations of the electron-diffraction patterns with the same [001] zone axis shown in Figure 5B and C. The domain block has an average width of around 200 nm, smaller than those observed in pure NN. The evident $\frac{1}{4}$ superlattice reflections confirm the presence of the antiferroelectric phase in this sample. The BF image in Figure 5D, obtained by selecting the direct beam and the surrounding $\frac{1}{4}$ superlattice reflections in the SAED pattern taken at the domain boundary, reveals the details of the APB structure (partly curved) as well as the annihilation of APBs. The irregular periodicity of APBs arrays is also visible, being consistent with the streaking feature in the SAED patterns. In addition, the domain boundary has a zig-zag character, denoted by the orange lines. Such zig-zag-shaped DB is commonly observed in ferroelectrics, which was suggested to act as a source of head-to-tail coupling to reduce the

electrostatic self-energy.⁵⁰⁻⁵² However, as pointed out earlier, the electrostatic energy in AFE is excluded due to the antipolarization nature of the structure. Thus, it is proposed that zig-zag-shaped DB in AFE serve as a way to gain mechanical compatibility and release mechanical stress. It is assumed that the nucleation of AFE domains occurs independently in different parts of the grain or near grain boundaries. When the domains with different antipolarization orientations get in contact, they form a domain boundary in a zig-zag shape to enable mechanical stress release. In a recent report, such zig-zag-shaped DB were found in PZ ceramics on the atomic scale to compensate for the unit cell shift caused by the APBs that had formed.⁴⁷ In general, the domain morphology and crystallography of pure NN are maintained in NN-0.03SS. The domain morphology is presented as a combination of both translational and orientational domains within one grain, including domain blocks with a smaller and more

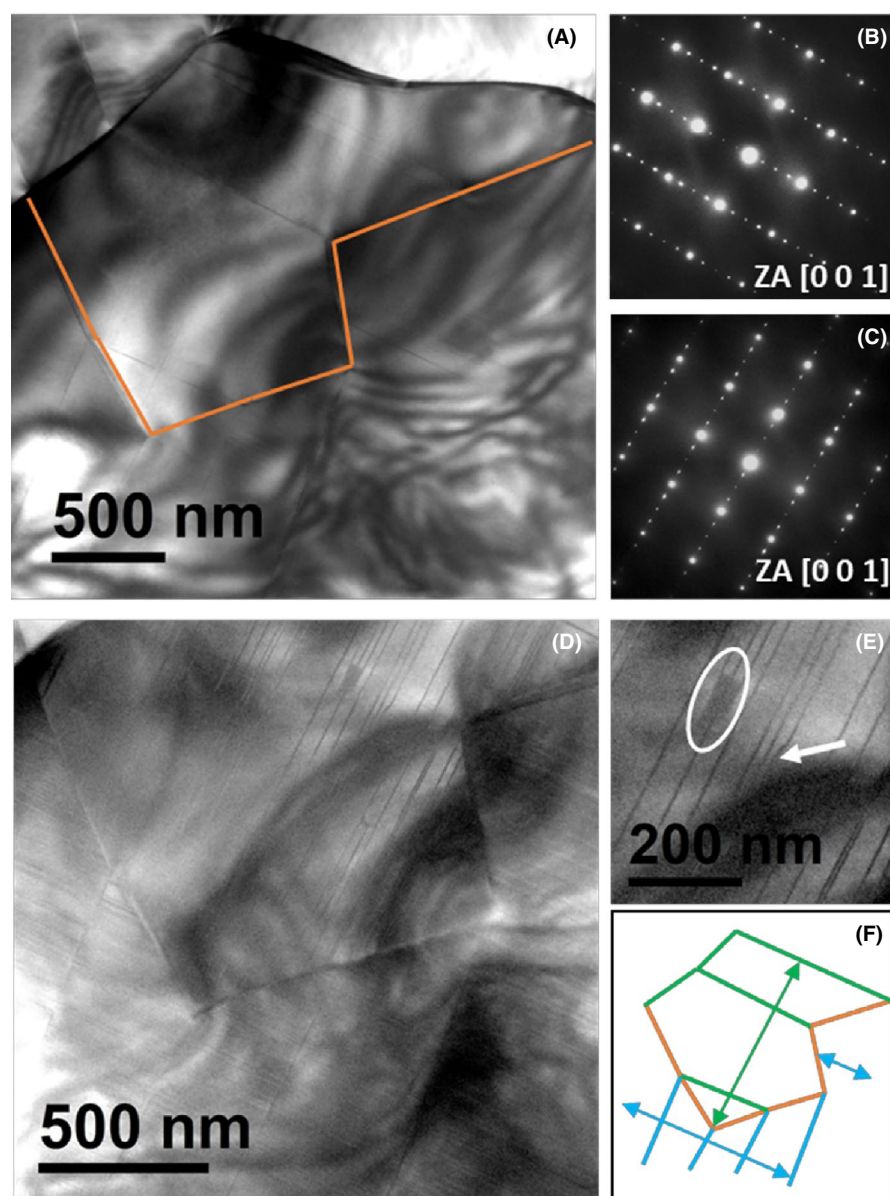


FIGURE 5 TEM characterization of the domain morphology and crystallography of NN-0.03SS solid solution. (A) BF imaging viewed along the $\langle 001 \rangle$ direction; corresponding SAED patterns shown in (B) and (C) for the upper left and lower right domain oriented along the [001] zone axis; (D) BF image obtained with direct beam and the surrounding $\frac{1}{4}$ and $\frac{1}{2}$ superlattice reflections in the SAED pattern taken right at the domain boundary; (E) the close-up image of the APBs (partly curved, denoted by the arrow) and the annihilation of APBs, denoted by the circle; (F) the schematic graph from this region, where the orange lines depict the zig-zag-shaped domain boundary and double arrows indicate the antipolarization vector of the different domains [Color figure can be viewed at wileyonlinelibrary.com]

homogeneously distributed size, as can be seen in the lower part of the grain. The APB arrays appear straight in pure NN but are partially curved in NN-0.03SS. Moreover, annihilation of APBs was also observed in this composition.

Figure 6 shows the characterization of NN-0.05SS. A defined and distinct domain structure with sharp domain boundaries is observed, as shown in Figure 6A-C, where domains are numbered for the following analysis of local twinning. We name this distinct morphology “parallelogram domains” due to the similarity in shape. The SAED pattern (Figure 6D) with $\frac{1}{4}$ superlattice reflections reveals readily the existence of antiferroelectricity. By selecting one of these $\frac{1}{4}$ superlattice reflection in the CDF image, APBs with line contrast of domain 3 were observed, as shown in Figure 6E. Based on the observed domain morphology, a schematic model was constructed from several images of this region, where the double-headed arrows denote the antipolarization vector in each domain; three domains are assigned accordingly. From this schematic graph, domain twinning can easily be demonstrated. It has to be noted that the electron-diffraction patterns in Figure 7B-D were recorded with a slightly different domain rotation with another zone axis [0 2 1]. It can be seen

that only domain 2 and domain 3 are tilted close to the zone axis [0 2 1], whereas domain 1 is not (as seen also by the domain contrast between domain 1 and 3). A slight flip of the reflection spots was observed in the SAED pattern upon crossing the domain boundary between domains 1 and 3, after carefully making sure that the spot splitting is not arising from the defocus of the beam. The ED pattern taken at the boundary between domains 1 and 3 is shown in Figure 7E, where the spot splitting is marked by the white circle. Since domains 2 and 3 have the same antipolarization directions, spot splitting is not observable in the corresponding SAED patterns. As previously observed in pure NN and NN-0.03SS, the domain block feature can also be found in NN-0.05SS. The parallelogram domains exhibit a very defined shape and form twins to reduce mechanical stress.

When more than 5% SrSnO₃ is introduced to NN, the hysteresis loop cannot be induced anymore due to the critical field of the AFE-FE transition exceeding the dielectric breakdown field.²⁴ The TEM investigation of NN-0.07SS is shown in Figure 8. The domain block feature is not observed any longer and the grains are likely to be occupied by one single domain, as shown in Figure 8A. Note that the observed

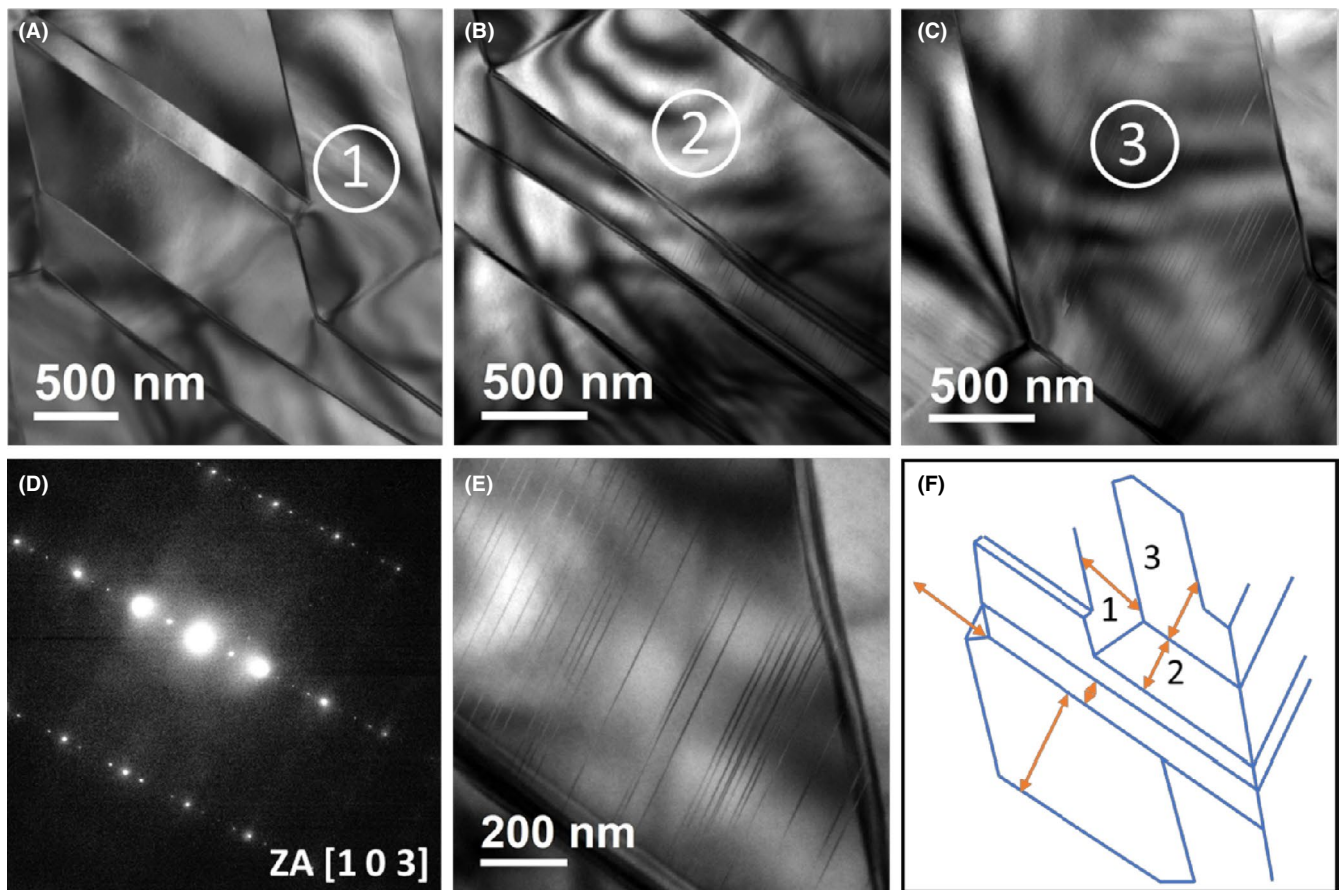


FIGURE 6 TEM characterization of the domain morphology and crystallography of one representative grain of NN-0.05SS solid solution. (A-C) BF images viewed along the $\langle 130 \rangle$ direction; (D) SAED pattern of this region; (E) CDF image, obtained with one of the $\frac{1}{4}$ superlattice reflections; (F) schematic model constructed based on several images from this region [Color figure can be viewed at wileyonlinelibrary.com]

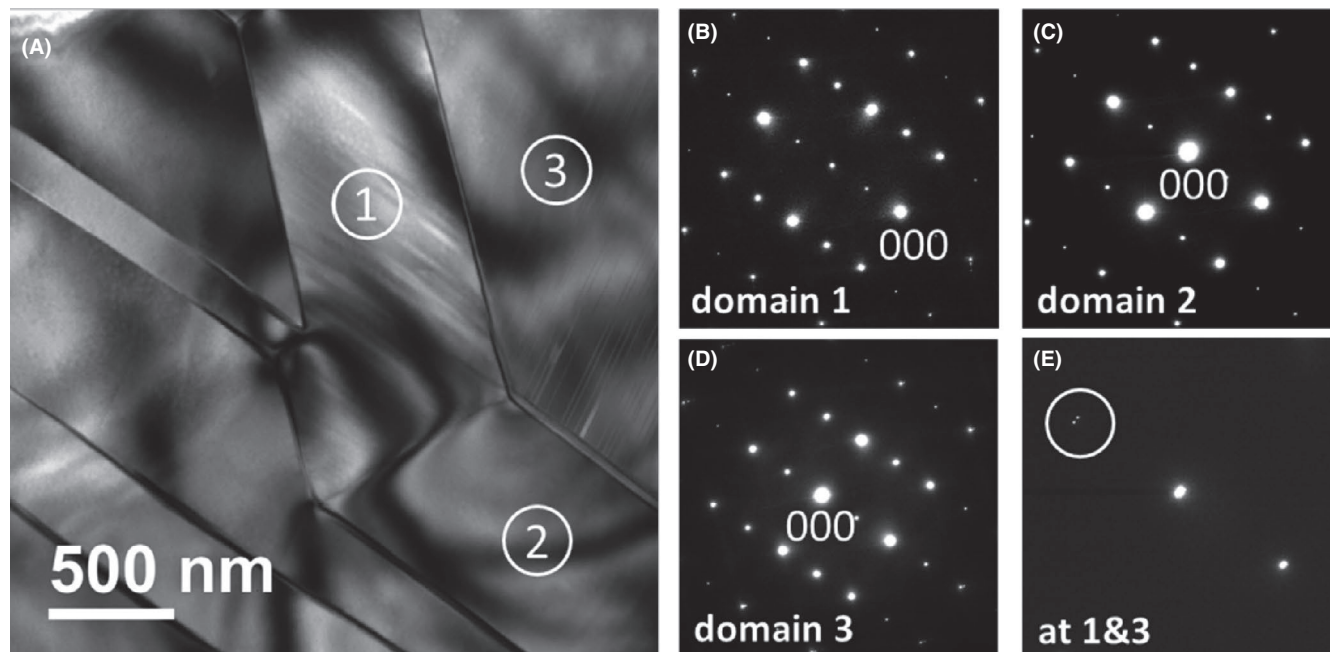


FIGURE 7 Twinning characterization of one region in NN-0.05SS. (A) The BF image of three neighboring domains; (B-D) the SAED patterns of domain 1, 2, and 3 with zone axis $[0\ 2\ 1]$, respectively (see also Figure 6); (E) the SAED pattern taken at the boundary between domain 1 and 3 (strongly enlarged)

thickness fringes in (A) indicate an inclined grain boundary, in this case at all interfaces to the adjacent grains. The examined grains are still of antiferroelectric nature, revealed by the $\frac{1}{4}$ superlattice reflections along with streaking features visible in the SAED pattern in Figure 8B. In the CDF image obtained with one of the $\frac{1}{4}$ superlattice reflections, APBs and dislocation loops⁵³ are revealed. Other defects such as secondary phases (SnO_2) and misfit and threading dislocations⁵⁴ are also introduced at this high incorporation level. It is assumed that the single domain grain morphology and the appearance of a considerable number of defects may be partially responsible for the lack of the respective double polarization hysteresis loops. Note that dislocations were previously demonstrated to interact with domain structures in ferroelectrics and influence the electromechanical properties.^{55,56} The absence of stress-compensating domain boundaries could also indicate a higher level of residual stresses in this sample, which additionally increases the critical AFE-FE transition field beyond the breakdown field; however, further experimental work is needed to clarify this hypothesis.

Overall, the domain morphology of pure NN is lost in NN-0.07SS, with single domain grains being characteristic of this composition. However, the antiferroelectricity is maintained, revealed by the characteristic $\frac{1}{4}$ superlattice reflections. The irregular periodicity of APBs persists at this composition and the resulting streaking feature becomes again more significant.

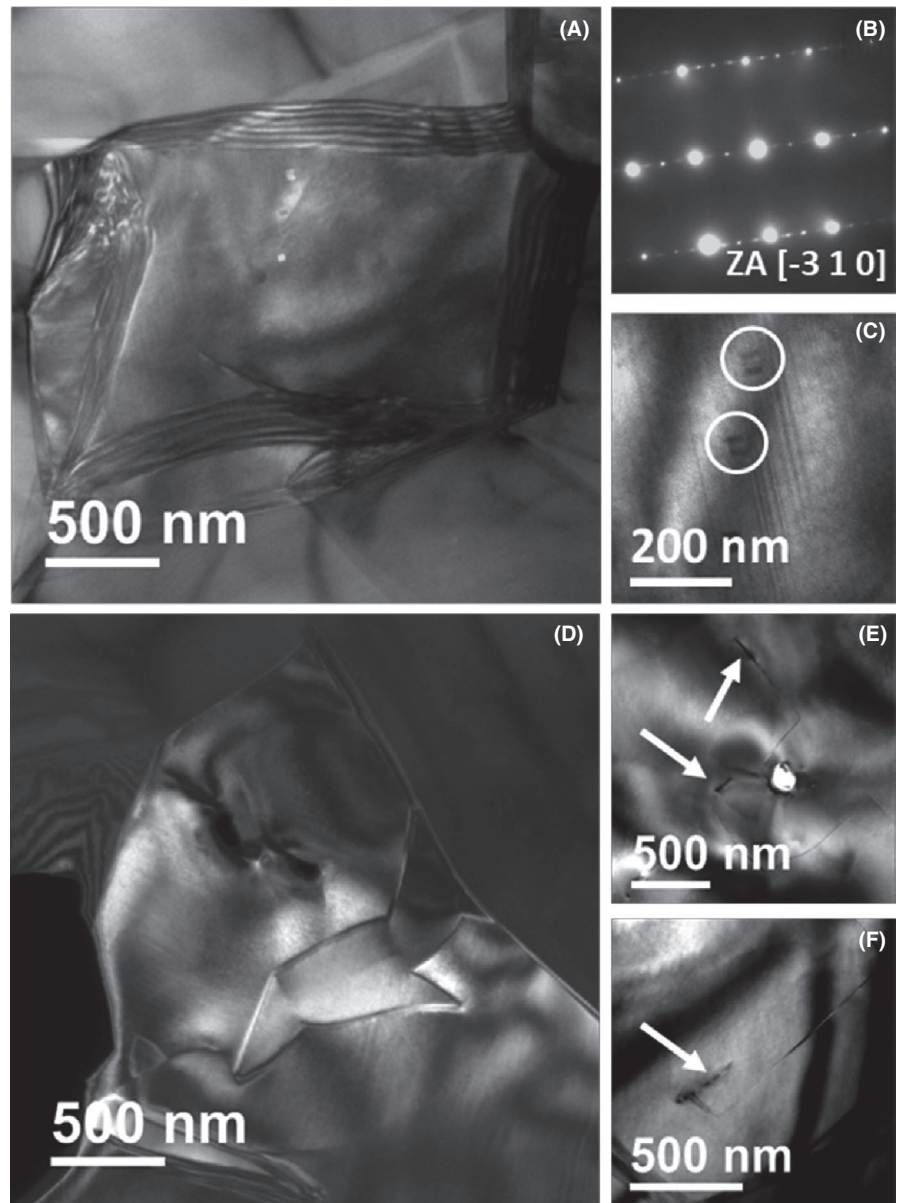
In this study, the NN-SS series has been systematically investigated by TEM. In the pure NN, the irregular periodicity

of APBs arrays is observed, associated with the lattice fringes and responsible for the streaking feature around $\frac{1}{4}$ superlattice reflections. This feature is maintained in all NN-SS series. The signature domain block is observed for low incorporation levels (up to 5%), but is absent in NN-0.07SS where the single domain occupies the entire grain. In particular, NN-0.05SS has demonstrated a very defined domain morphology with parallelogram domains.

The symmetry of the P phase with the P₆mm space group is preserved in the entire NN-SS series, which was confirmed by the observation of the characteristic $\frac{1}{4}$ superlattice reflections in all the investigated compositions, independent of the incorporation level of SrSnO_3 . This behavior contrasts the reported behavior in PZ-based modified materials, where both the domain morphology and the resulting crystal structures are strongly compositional dependent.⁵⁷

It can be concluded that the substitution of Sr and Sn into NaNbO_3 leads to a significant change in the domain structures, whereas the antiferroelectricity is preserved. Moreover, a previous study has shown that although the global crystallographic structure is preserved, this substitution increases the unit cell volume and induces large changes in the local disorder on the Na sites.²⁴ The intrinsic changes in the structure as well as the extrinsic contribution from the domain structure could be responsible for the observed change of the irreversible AFE-FE transition in pure NN into a reversible one in NN-SS. However, distinguishing these contributions requires further investigations using advanced in situ characterization methods.

FIGURE 8 TEM characterization of the domain morphology and crystallography of NN-0.07SS solid solution. (A) BF image of one representative grain; (B) SAED pattern recorded along the $[-310]$ zone axis; (C) CDF image obtained by selecting one of the $\frac{1}{4}$ superlattice reflection, where the circles denote two dislocation loops; (D) the domain morphology of another representative grain; (E, F) the close-up images of dislocations present in this sample, which are marked by arrows



4 | CONCLUSIONS

A $(1-x)\text{NaNbO}_3\text{-}x\text{SrSnO}_3$ solid solution series was systematically investigated by TEM, focusing on the domain morphology and crystallography, that is, the resulting crystal structures after chemical modification. It was confirmed that antiferroelectricity is maintained in all the investigated compositions, revealed by the characteristic AFE electron-diffraction patterns. The lines with dark contrast are clarified to be APBs, whose irregular periodicity is responsible for the streaking features around the $\frac{1}{4}$ superlattice reflections. The signature domain block of pure NN is preserved in the NN-SS series, with the exception of NN-0.07SS. In particular, a well-defined and distinct domain configuration is observed in NN-0.05SS, including a parallelogram domain morphology.

ACKNOWLEDGMENTS


The authors are greatly indebted to the LOEWE collaborative project FLAME (Fermi level engineering of anti-ferroelectric materials for energy storage and insulation systems) supported by the Hessian State Ministry for Higher Education, Research and the Arts. H.D. and L.M.-L. acknowledge financial support from the European Research Council (ERC) “Horizon 2020” Program under grant no. 805359-FOXON. Open access funding enabled and organized by Project DEAL.

ORCID

Hui Ding  <https://orcid.org/0000-0001-5722-0053>

Mao-Hua Zhang  <https://orcid.org/0000-0002-9823-4547>

Jurij Koruza  <https://orcid.org/0000-0002-0258-6709>

Leopoldo Molina-Luna  <https://orcid.org/0000-0002-9412-8093>

REFERENCES

- Dougherty JP. Cardiac defibrillator with high energy storage anti-ferroelectric capacitor. U.S. Patent 5, 545, 184, 1996.
- Mischenko AS, Zhang Q, Scott JF, Whatmore RW, Mathur ND. Giant electrocaloric effect in thin-film $\text{PbZr}_{0.95}\text{Ti}_{0.05}\text{O}_3$. *Science*. 2006;311(5765):1270–1.
- Novak N, Weyland F, Patel S, Guo H, Tan X, Rödel J, et al. Interplay of conventional with inverse electrocaloric response in (Pb, Nb) (Zr, Sn, Ti) O_3 antiferroelectric materials. *Phys Rev B*. 2018;97(9):094113.
- Kittel C. Theory of antiferroelectric crystals. *Phys Rev*. 1951;82(5):729–32.
- Shirane G. Ferroelectricity and antiferroelectricity in ceramic PbZrO_3 containing Ba or Sr. *Phys Rev*. 1952;86(2):219–27.
- Haertling GH, Land CE. Hot-pressed (Pb, La)(Zr, Ti) O_3 ferroelectric ceramics for electrooptic applications. *J Am Ceram Soc*. 1971;54(1):1–11.
- Fesenko OE, Kolesova RV, Sindeyev YUG. The structural phase transitions in lead zirconate in super-high electric fields. *Ferroelectrics*. 1978;20(1):177–8.
- Xu Z, Viehland D, Yang P, Payne DA. Hot-stage transmission electron microscopy studies of phase transformations in tin-modified lead zirconate titanate. *J Appl Phys*. 1993;74(5):3406–13.
- Rödel J, Jo W, Seifert KTP, Anton E-M, Granzow T, Damjanovic D. Perspective on the development of lead-free piezoceramics. *J Am Ceram Soc*. 2009;92(6):1153–77.
- Tan X, Ma C, Frederick J, Beckman S, Webber KG. The antiferroelectric \leftrightarrow ferroelectric phase transition in lead-containing and lead-free perovskite ceramics. *J Am Ceram Soc*. 2011;94(12):4091–107.
- EU-Directive 2002/95/EC: Restriction of the use of certain hazardous substances in electrical and electronic equipment (RoHS). *J Eur Union*. 2006;46(L37):24–38.
- Matthias BT. New ferroelectric crystals. *Phys Rev*. 1949;75(11):1771.
- Vousden P. The structure of ferroelectric sodium niobate at room temperature. *Acta Cryst*. 1951;4(6):545–51.
- Cross LE, Nicholson BJLV. The optical and electrical properties of single crystals of sodium niobate. *J Sci*. 1955;46(376):453–66.
- Megaw HD, Wells M. The space group of NaNbO_3 and $(\text{Na}_{0.995}\text{K}_{0.005})\text{NbO}_3$. *Acta Cryst*. 1958;11(12):858–62.
- Wood EA, Miller RC, Remeika JP. The field-induced ferroelectric phase of sodium niobate. *Acta Cryst*. 1962;15(12):1273–9.
- Koruza J, Tellier J, Malič B, Bobnar V, Kosec M. Phase transitions of sodium niobate powder and ceramics, prepared by solid state synthesis. *J Appl Phys*. 2010;108(11):113509.
- Glazer AM, Megaw HD. Studies of the lattice parameters and domains in the phase transitions of NaNbO_3 . *Acta Cryst A*. 1973;29(5):489–95.
- Zhang M-H, Fulanović L, Egert S, Ding H, Groszewicz PB, Kleebe H-J, et al. Electric-field-induced antiferroelectric to ferroelectric phase transition in polycrystalline NaNbO_3 . *Acta Mater*. 2020;200:127–35.
- Koruza J, Groszewicz P, Breitzke H, Buntkowsky G, Rojac T, Malič B. Grain-size-induced ferroelectricity in NaNbO_3 . *Acta Mater*. 2017;126:77–85.
- Zhelnova OA, Fesenko OE. Phase transitions and twinning in NaNbO_3 crystals. *Ferroelectrics*. 1987;75(1):469–75.
- Li W, Xia X, Zeng J, Zheng L, Li G. Significant differences in NaNbO_3 ceramics fabricated using Nb_2O_5 precursors with various crystal structures. *Ceram Int*. 2020;46(3):3759–66.
- Shimizu H, Guo H, Reyes-Lillo SE, Mizuno Y, Rabe KM, Randall CA. Lead-free antiferroelectric: CZ_NN ($0 \leq X \leq 0.10$). *Dalton Trans*. 2015;44(23):10763–72.
- Zhang M-H, Hadaeghi N, Egert S, Ding H, Zhang H, Groszewicz PB, et al. Design of lead-free antiferroelectric $(1-x)\text{NaNbO}_3-x\text{SrSnO}_3$ compositions guided by first-principles calculations. *Chem Mater*. 2021;33(1):266–74.
- Guo H, Shimizu H, Randall CA. Microstructural evolution in NaNbO_3 -based antiferroelectrics. *J Appl Phys*. 2015;118(17):174107.
- Gao L, Guo H, Zhang S, Randall CA. A perovskite lead-free antiferroelectric CH_NN with induced double hysteresis loops at room temperature. *J Appl Phys*. 2016;120(20):204102.
- Wood EA. Polymorphism in potassium niobate, sodium niobate, and other ABO_3 compounds. *Acta Cryst*. 1951;4(4):353–62.
- Shirane G, Newnham R, Pepinsky R. Dielectric properties and phase transitions of NaNbO_3 and $(\text{Na}, \text{K})\text{NbO}_3$. *Phys Rev*. 1954;96(3):581–8.
- Jona F, Shirane G, Pepinsky R. Optical study of PbZrO_3 and NaNbO_3 single crystals. *Phys Rev*. 1955;97(6):1584–90.
- Dec J. Real domain structure in orthorhombic phase of NaNbO_3 crystals. *Cryst Res Technol*. 1983;18(2):195–204.
- Chen J, Feng D. TEM study of phases and domains in NaNbO_3 at room temperature. *Phys Stat Sol (a)*. 1988;109(1):171–85.
- Chen J, Feng D. In situ TEM studies of para—Ferro phase transitions in NaNbO_3 . *Phys Stat Sol (a)*. 1988;109(2):427–34.
- Zhelnova OA, Raevski IP, Reznichenko LA. Microstructure, domain structure and phase-transition behavior of alkali niobate-based materials with varying conductivity. *Ferroelectr Lett Sect*. 1990;11(3):57–62.
- Gao L, Guo H, Zhang S, Randall CA. Stabilized antiferroelectricity in BS-NN lead-free ceramics with established double hysteresis loops. *Appl Phys Lett*. 2018;112(9):092905.
- Zheludev IS. Domain structure of ferroelectrics and antiferroelectrics. In: Tybulewicz A, editor. *Physics of crystalline dielectrics vol. 1 crystallography and spontaneous polarization*, 1st edn. New York/London: Plenum Press; 1971. p. 149–204.
- Xu Z, Dai X, Viehland D. Incommensuration in La-modified antiferroelectric lead zirconate titanate ceramics. *Appl Phys Lett*. 1994;65(25):3287–9.
- He H, Tan X. In situ transmission electron microscopy study of the electric field-induced transformation of incommensurate modulations in a Sn-modified lead zirconate titanate ceramic. *Appl Phys Lett*. 2004;85(15):3187–9.
- Guo H, Shimizu H, Randall CA. Direct evidence of an incommensurate phase in NaNbO_3 and its implication in NaNbO_3 -based lead-free antiferroelectrics. *Appl Phys Lett*. 2015;107(11):112904.
- Xu Z, Dai X, Viehland D. Impurity-induced incommensuration in antiferroelectric La-modified lead zirconate titanate. *Phys Rev B*. 1995;51(10):6261–71.
- Sakowski-Cowley AC, Łukaszewicz K, Megaw HD. The structure of sodium niobate at room temperature, and the problem of reliability in pseudosymmetric structures. *Acta Cryst*. 1969;25(5):851–65.
- Glazer AM. Simple ways of determining perovskite structures. *Acta Cryst A*. 1975;31(6):756–62.
- de Graef M, Speck JS, Clarke DR, Dimos D. Electron microscopic study of domains in relaxor ferroelectrics. *MRS Proc*. 1992;243:3–14.
- Chang Y-J, Lian J-Y, Wang Y. One-dimensional regular arrays of antiphase domain boundaries in anti-ferroelectric PNZST ceramics. *Appl Phys A*. 1985;36(4):221–7.

44. Baba-Kishi KZ, Barber DJ. Transmission electron microscope studies of phase transitions in single crystals and ceramics of ferroelectric $\text{Pb}(\text{Sc}_{1/2}\text{Ta}_{1/2})\text{O}_3$. *J Appl Cryst*. 1990;23(1):43–54.
45. Amelinckx S, Van Landuyt J. Contrast effects at planar interfaces. In: Wenk HR, editor. *Electron microscopy in mineralogy*. Springer-Verlag Berlin Heidelberg New York; 1976. p. 68–112.
46. Wei X-K, Tagantsev AK, Kvasov A, Roleder K, Jia C-L, Setter N. Ferroelectric translational antiphase boundaries in nonpolar materials. *Nat Commun*. 2014;5(1):3031.
47. Ma T, Fan Z, Tan X, Zhou L. Atomically resolved domain boundary structure in lead zirconate-based antiferroelectrics. *Appl Phys Lett*. 2019;115(12):122902.
48. Arlt G. Twinning in ferroelectric and ferroelastic ceramics: stress relief. *J Mater Sci*. 1990;25(6):2655–66.
49. Lines M, Glass A. *Principles and applications of ferroelectrics and related materials*. Oxford: Clarendon Press; 1977. p. 87–128.
50. Randall CA, Barber DJ, Whatmore RW. Ferroelectric domain configurations in a modified-PZT ceramic. *J Mater Sci*. 1987;22(3):925–31.
51. Demczyk BG, Rai RS, Thomas G. Ferroelectric domain structure of lanthanum-modified lead titanate ceramics. *J Am Ceram Soc*. 1990;73(3):615–20.
52. Ricote J, Whatmore RW, Barber DJ. Studies of the ferroelectric domain configuration and polarization of rhombohedral PZT ceramics. *J Phys Condens Matter*. 2000;12(3):323–37.
53. Suzuki T, Ueno M, Nishi Y, Fujimoto M. Dislocation loop formation in nonstoichiometric $(\text{Ba}, \text{Ca})\text{TiO}_{1/2}$ and $\text{BaTiO}_{1/2}$ ceramics. *J Am Ceram Soc*. 2001;84(1):200–6.
54. Liu XW, Hopgood AA, Usher BF, Wang H, Braithwaite NSJ. Formation of misfit dislocations during growth of $\text{In}_x\text{Ga}_{1-x}\text{As}/\text{GaAs}$ strained-layer heterostructures. *Semicond Sci Technol*. 1999;14(12):1154–60.
55. Kotsos A, Landis CM. Computational modeling of domain wall interactions with dislocations in ferroelectric crystals. *Int J Solids Struct*. 2009;46(6):1491–8.
56. Ren P, Höfling M, Koruza J, Lauterbach S, Jiang X, Frömling T, et al. High temperature creep-mediated functionality in polycrystalline barium titanate. *J Am Ceram Soc*. 2020;103(3):1891–902.
57. Schmitt LA, Schönau KA, Theissmann R, Fuess H, Kungl H, Hoffmann MJ. Composition dependence of the domain configuration and size in $\text{Pb}(\text{Zr}_{1-x}\text{Ti}_x)\text{O}_3$ ceramics. *J Appl Phys*. 2007;101(7):074107.

SUPPORTING INFORMATION

Additional supporting information may be found online in the Supporting Information section.

How to cite this article: Ding H, Zhang M-H, Koruza J, Molina-Luna L, Kleebe H-J. Domain morphology of newly designed lead-free antiferroelectric NaNbO_3 - SrSnO_3 ceramics. *J Am Ceram Soc*. 2021;104:3715–3725. <https://doi.org/10.1111/jace.17738>